

## RESEARCH ARTICLE Water renewals in the Saguenay Fjord

10.1002/2015JC011085

Mélany Belzile<sup>1</sup>, Peter S. Galbraith<sup>2</sup>, and Daniel Bourgault<sup>1</sup>

## Key Points:

- Fjord renewal dynamics strongly dependent on St. Lawrence Estuary seasonality
- Three renewal regimes, linked to seasonality, showing large interannual variability
- Internal wave breaking may be a significant contributor to deep mixing

## Correspondence to:

M. Belzile,  
melany\_belzile@uqar.ca

## Citation:

Belzile, M., P. S. Galbraith, and D. Bourgault (2015), Water renewals in the Saguenay Fjord, *J. Geophys. Res. Oceans*, 120, doi:10.1002/2015JC011085.

Received 29 JUN 2015

Accepted 16 DEC 2015

Accepted article online 18 DEC 2015

<sup>1</sup>Institut des sciences de la mer de Rimouski, Rimouski, Quebec, Canada, <sup>2</sup>Department of Fisheries and Oceans Canada, Maurice Lamontagne Institute, Mont-Joli, Quebec, Canada

**Abstract** Water renewals and renewal times of the Saguenay Fjord are investigated and classified according to their intrusion depth. Renewal dynamics are controlled by a shallow sill (~20 m) at the fjord mouth, by large tides that are a distinguishing feature of the Saguenay Fjord and by large vertical mixing inside the inner basin ( $K \sim 10^{-4} \text{ m}^2 \text{ s}^{-1}$ ). A mooring was deployed in the inner basin of the fjord to provide a clearer quantitative understanding of the complexity and seasonality of water renewals in this seasonally ice-covered fjord. The mooring provided information on currents over nearly the entire water column, along with temperature-salinity at a few discrete depths. Hydrographic temperature and salinity transects spanning multiple seasons and years as well as turbulence profiles were also collected. The observations show that the fjord dynamics are more complex than previously hypothesized, with large changes in renewal event depths leading to three different renewal regimes. Part of this renewal depth variability may be explained by the seasonality of the St. Lawrence estuarine circulation. Because of the large turbulence within the inner basin bottom layer, the density decreases over time such that new deep renewals can occur every year. The mechanisms behind the large vertical mixing cannot yet be clearly identified but a statistically significant correlation ( $K \propto N^{-1.3}$ ) suggests that internal wave breaking may be a significant contributor to deep turbulence mixing in the inner basin. The renewal time of the inner basin waters is estimated to be between 1 and 6 months.

## 1. Introduction

### 1.1. Saguenay Fjord

Fjords are generally characterized by sills which can limit the exchanges between internal and external waters [Allen and Simpson, 1998]. The weak dynamics associated with some deep fjords may induce stagnation periods promoting low oxygen zones [Farmer and Freeland, 1983]. In other cases, such as in the Saguenay Fjord, energetic tides can regularly drive dense external waters over sills and into the basins. This generally produces strong turbulent mixing at sills that can ventilate the dense intruding waters with well-oxygenated near surface waters [Farmer and Freeland, 1983]. The deep water renewals of such fjords are therefore generally well oxygenated.

The Saguenay Fjord (Figure 1), located in the subarctic region of eastern Canada, is the southernmost fjord of the Northern Hemisphere to be seasonally ice covered. The fjord is 110 km long, 2.0 km wide on average with a mouth width of 1.1 km, has two upstream arms, three major sills, two outer basins, a large inner basin of 280 m depth occupying two thirds of its total length and a total volume of 41 km<sup>3</sup>. The first sill, located at the mouth, near Tadoussac, has a depth of 20 m. The other two sills, located 18 and 32 km upstream, have depths of 60 and 115 m and widths of 2.0 and 1.7 km, respectively.

The shallow sill at the fjord's entrance controls the overall dynamics and plays an important role in advective and diffusive transport processes in the deep inner basin. Its shallow depth acts as a barrier for deep estuarine water. Consequently, the fjord can only receive dense estuarine waters that have been tidally upwelled, at the head of the Laurentian channel, sufficiently far up against the seaward side of the sill to make it over. This barotropic process is called aspiration and is a common feature to all fjords [Nall and Gillibrand, 2010]. Because of the funneling geometry of the St. Lawrence Estuary, tidal ranges are quite large at the fjords mouth (4 m on average, increasing to roughly 6 m during spring tides) [Seibert et al., 1979] compared with other fjords that flow directly into the ocean [Bélanger, 2003]. Given the strong tidal currents

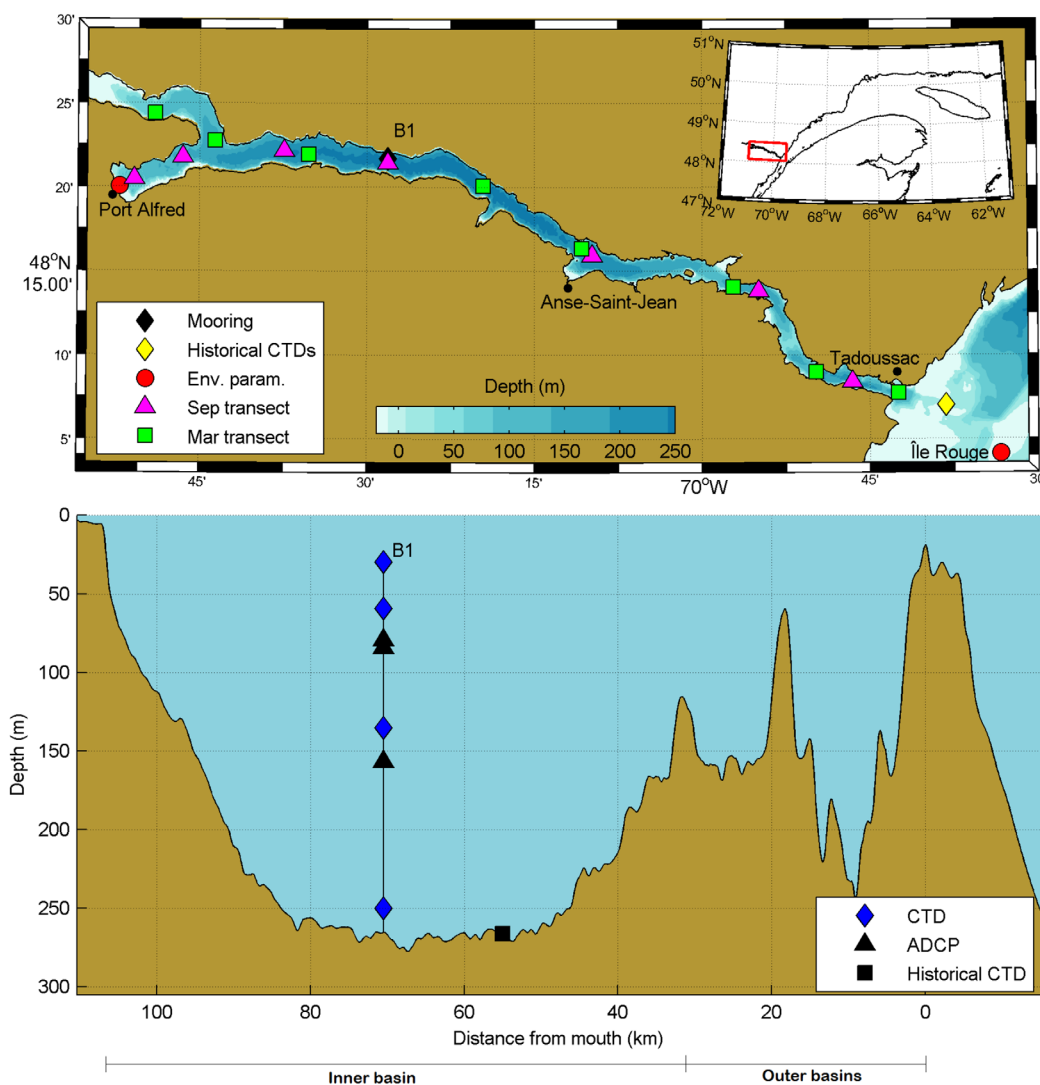


**Figure 1.** (top) Map of the Saguenay bathymetry showing examples of CTD stations (pink triangles are September 2011 stations and green squares are March 2012 stations) and mooring B1 location (black diamond). Weather station and tide gauge (red circles) are also on the map along with a historical moored CTDs at the sill (yellow diamonds). (bottom) Longitudinal section showing location of moored instruments (black square is historical CTD of *Bélanger* [2003]).

at the mouth of the Saguenay, the maximum upward displacement can reach 100 m at the sill [*Lavoie et al.*, 2000] and the inward volume flux per tide cycle is estimated at  $0.8 \text{ km}^3$  [*Therriault et al.*, 1984].

The large seasonal variability of the density of the upwelled water largely dictates renewal depths [*Gade*, 1986]. As it is common in fjords, density is mainly a function of salinity [*Allen and Simpson*, 1998; *Cottier et al.*, 2010]. Therefore, the salinity of the topmost 100 m of the adjacent estuary is of great significance for the dynamics of the Saguenay Fjord. In winter, the water column of the St. Lawrence Estuary is divided in two layers, a near-freezing mixed surface layer and a warmer saltier layer underneath, while in summer the Estuary is characterized by three layers, a warm surface layer, a cold intermediate layer (CIL) and a warmer and saltier bottom layer [*Galbraith*, 2006].

Another important factor controlling the circulation is the strong mixing associated with sill processes (breaking lee waves, internal hydraulic jumps, shear instabilities, etc.) [*Geyer and Cannon*, 1982; *Farmer and Freeland*, 1983; *Saucier and Chassé*, 2000; *Janes*, 2008; *Baschek and Jenkins*, 2009; *Stacey and Gratton*, 2001; *Cyr et al.*, 2015]. Consequently, the deep fjord waters in all three basins are well oxygenated [*Drainville*, 1968; *Taylor*, 1975; *Therriault and Lacroix*, 1975]. This mixing process greatly influences the buoyant depth at

which the intruding water will spread within the inner basin of the fjord [Geyer and Cannon, 1982; Farmer and Freeland, 1983]. Once the intrusion has passed the sill turbulence, mixing inside the basin further decreases its density, eventually permitting new deep renewal events to occur. This mixing can arise during renewal events from entrainment of resident water with the density-driven plume [Liungman et al., 2001; Arneborg et al., 2004a], or in periods of stagnation, from vertical diffusion possibly induced by internal waves [Stigebrandt and Aure, 1989; Inall and Rippeth, 2002]. Seibert et al. [1979] hypothesized that the action of internal waves was responsible for the short replacement period in the outer basin of the Saguenay (1–3 days) [Therriault et al., 1984]. The total energy flux into the Saguenay is estimated to be 56 MW from the modeling work of Stacey and Gratton [2001]. Most of this energy is dissipated (bottom and sidewall friction account for ~24 MW of dissipation, while the horizontal and vertical diffusion account for ~17 MW of dissipation) and the residual goes into mixing in the outer basin (15 MW).

The Saguenay River is the most important tributary to the Saguenay Fjord and the second in importance to the St. Lawrence Estuary with a mean fresh water discharge of  $\sim 1200 \text{ m}^3 \text{ s}^{-1}$  (1944–1993) [Bélanger, 2003]. The river outflow has been regulated by dams since 1926. The freshwater runoff induces a sharp halocline, often conveniently used to separate the two major water masses of the fjord, and to describe the fjord circulation as estuarine: a thin (5–10 m) brackish ( $S \sim 10$ ) surface layer and a compensating saltier ( $S \sim 30$ ) bottom layer [Drainville, 1968; Loucks and Smith-Sinclair, 1975; Therriault and Lacroix, 1975; Therriault et al., 1984]. However, in deep fjords, the estuarine circulation only affects the near-surface circulation and does not drive the circulation far below the main pycnocline [Gade and Edwards, 1980; Mortensen et al., 2014]. The vertical structure and the residual circulation of the Saguenay are in fact far more complex than this two-layer idealization and rather consist of multiple inflowing as well as outflowing layers of various origins [Stacey and Gratton, 2001; Bélanger, 2003; Bourgault et al., 2012a]. Mortensen et al. [2014] have simplified complex seasonal dynamics of subarctic fjords as a combination of four circulation modes. Based on the definitions of these modes, the Saguenay is mostly characterized by the estuarine circulation mode (driven by freshwater runoff) and by the dense coastal inflow mode (driven by density differences between coastal and fjord waters).

### 1.2. Early Hypotheses and Current Understanding on Renewal Origin

Drainville [1968] proposed two hypotheses for the origin of the deep Saguenay water. The first was that the bottom waters originate from St. Lawrence Estuary superficial water. His second hypothesis was that the bottom waters of the fjord may also originate from local deep winter convection as seen in arctic fjords by brine rejection [Cottier et al., 2010]. Two studies rejected the latter hypothesis [Loucks and Smith-Sinclair, 1975; Bourgault et al., 2012a]. It is now accepted that the renewal of the inner basin arises from water advected from the St. Lawrence Estuary waters mixed with Saguenay waters [Loucks and Smith-Sinclair, 1975; Therriault and Lacroix, 1975; Seibert et al., 1979; Therriault et al., 1984; Schafer et al., 1990; Baschek and Jenkins, 2009; Bourgault et al., 2012a; Xie et al., 2012]. Xie et al. [2012] used chromophoric dissolved organic matter (CDOM) as a physical tracer to find that 94% of the inner basin deep waters came from the CIL and 6% was supplied by the Saguenay River.

Based on sudden density increases measured from a temperature-salinity (T-S) probe at the bottom of the inner basin ( $\sim 260 \text{ m}$ , black square in Figure 1), Bélanger [2003] identified 12 deep renewal events between August 1998 and January 1999 with the greatest density changes occurring in December and January. Four of the deep renewals occurred during the summer, in August, and the remaining eight occurred in fall and winter. Based on his interpretation, these renewals pushed the previous resident winter waters upward and up-fjord which eventually increased the density in the entire inner basin. Deep intrusions were preceded by intrusions without sufficient density to reach the seafloor and therefore occurred at intermediate depths within the inner basin. This middepth warm layer was observed in other studies and shows a high variability in terms of thickness (40–100 m), depth (centered at 40–95 m depth) and temperature (1–4°C) [Drainville, 1968; Taylor, 1975; Sundby and Loring, 1978; Seibert et al., 1979; Bélanger, 2003; Bourgault et al., 2012a].

As mentioned previously, the two major factors controlling the dynamics of deep renewal events are advection at the entrance sill and mixing rates at sills and within the fjord. Nonetheless, depending on the season, other environmental controlling factors can be important. Bélanger [2003] identified wind direction as having a significant role in summer. His observations and simulations showed that the presence of north-easterly winds could prevent summer deep renewals because the wind piles up fresh water near the

**Table 1.** Instrumental Details of Mooring B1<sup>a</sup>

Depth of the Instrument (m)	Instrument Type	Brand	Model	Sampling Interval (min)
30 ± 3	CTD	Sea-Bird	SBE 37	10
59 ± 3	CTD	Sea-Bird	SBE 37	5
79 ± 3	ADCP	RD Instruments	WH-S-300khz	30
84 ± 3	ADCP	RD Instruments	WH-S-300khz	30
135 ± 3	CTD	Sea-Bird	SBE 37	5
157 ± 0	ADCP	RD Instruments	WH-S-300khz	30
250 ± 3	CTD	Sea-Bird	SBE 37	5

<sup>a</sup>Instrument depths are averages  $\pm 2\sigma$  (where  $\sigma$  is the standard deviation).

shallow sill and decelerates the outflow from the Saguenay. Moreover, the autumn-winter renewal events occurred more or less on a fortnightly cycle which suggests that they were controlled by the neap-spring tide modulation [Lavoie *et al.*, 2000; Bélanger, 2003].

By interpreting and comparing summer and winter T-S properties, Bourgault *et al.* [2012a] proposed two hypotheses that would define the seasonality of the Saguenay renewals. They hypothesized that the winter temperature field is composed of a warm intermediate layer, which they called Saguenay Intermediate Water (SIW), located between 20 and 60 m, that would be the remains of a thicker and warmer summer layer. It is important to note that the SIW is initially driven by barotropic tidal exchange unlike the typical intermediate water found in deep sill fjords which is driven by baroclinic pumping above sill depth [e.g., Stigebrandt, 1990; Inall and Gillibrand, 2010; Stigebrandt, 2012; Sciascia *et al.*, 2014; Sutherland *et al.*, 2014; Mortensen *et al.*, 2014]. The SIW would be formed during the previous summer from a mixture of surface fjord waters and St. Lawrence Estuary CIL water that had made its way over the shallow sill of the fjord. This layer would be displaced upward and would become partially eroded over the winter season. They further hypothesized this winter erosion to be caused by the mixing of this layer (SIW) over the sills with very cold water from the St. Lawrence Estuary. The new mixture forms the Saguenay Deep Water (SDW). This salty and very cold water would be sufficiently dense to dive and displace the resident deep waters.

As presented above, the circulation in the inner basin of the Saguenay Fjord is particularly complex and our understanding was solely based on either interpretation of T-S structure and diagrams or numerical models. To our knowledge, no measurements of currents or mixing were available to test ideas, hypotheses, and model results about the residual circulation, its seasonal evolution, and diffusion mechanisms.

### 1.3. Objectives

The main goal of the present work is to provide a clearer quantitative understanding of the complexity and seasonality of water renewals in this seasonally ice-covered fjord. In order to achieve this objective, we will test the two hypotheses about the seasonality of the intermediate and deep circulations [Bourgault *et al.*, 2012a] with year-long current measurements. The secondary objective is to quantify the inner basin renewal time and diffusive mixing.

## 2. Data Sets and Methodology

A mooring (B1) was deployed in 2011–2012 to collect long-term time series of physical properties and currents in the inner basin of the Saguenay Fjord (Figure 1). The details of the moored instruments are presented in Table 1. Additionally, nine hydrographic CTD surveys were made between 2010 and 2013 along the fjord (Figure 1) and new turbulence profiles were collected near Anse-Saint-Jean in February 2011.

### 2.1. Mooring

Mooring B1 was deployed in the inner basin at 48°21.494'N 070°28.128'W from the research vessel *Coriolis II* on 18 September 2011. The mooring included a series of three acoustic Doppler current profilers (ADCPs), which together provided 2 m resolution current data over most of the water column, as well as four T-S sensors (CTD) at fixed depths. All instruments sampled until the recovery date, 16 July 2012, except for the CTD moored at 250 m depth which stopped on 9 July 2012. Moreover, the shallower CTD moored at 30 m depth failed to record salinity.

Data quality control was completed on the ADCP data by Québec-Océan [Guillot, 2011]. Briefly, a series of tests was carried out to flag unphysical or suspicious values of temperature, pressure, and velocity. The procedure was derived from the toolbox ADCPtools released by the U.S. Geological Survey to which additional tests were added for ADCPs mounted on mooring lines. The tests were based on expected pressure or temperature ranges and on parameters returned by the ADCPs (e.g., echo intensity, magnitude correlation, error velocity, and percentage good). The velocity coordinate system was rotated along the fjord axis (i.e., clockwise rotation of 10°). The temperature, salinity, and current data were then interpolated onto a regular grid. Temporal linear interpolation (every 30 min) followed by a vertical linear interpolation (every 2 m) was chosen over triangle-based bilinear interpolation, which provided unrealistic interpolations. To highlight the low-frequency seasonal circulation, the data were low-pass filtered to remove frequencies equal to or higher than the spring-neap cycle, using a nonrecursive Hamming-window filter with a cutoff period of 15 days.

### 2.2. CTD Surveys

Wintertime hydrographic T-S transect data were collected by an airborne Canadian Coast Guard Bell-212 helicopter using a Sea-Bird SBE19plus, covering both the open water and ice-covered portions of the fjord and complementing summertime data obtained by boat. While the winter transects were part of a larger survey which has taken place throughout the Gulf of St. Lawrence every March since 1996 (Galbraith [2006], updated in annual reports, e.g., Galbraith *et al.* [2015]), March 2011 was the first time the survey extended into the Saguenay Fjord. The ice-free hydrographic surveys were mostly collected using a Sea-Bird SBE911-plus onboard of the research vessel *Coriolis II* as well as a Sea-Bird SBE19plus deployed from Canadian Department of Fisheries and Oceans (DFO) small craft boats. The October transect was collected by the Saguenay-St. Lawrence Marine Park. It should be noted that the two westernmost stations of the September transects were located in the southern arm of the fjord unlike the March transects when the stations were located in the northern arm (Figure 1).

The SBE19 and SBE37 calibrations were done prior to deployment and verified postdeployment by the manufacturer. The SBE19 used for winter transects had their calibrations verified before and after deployment in a temperature-controlled bath at multiple temperatures and salinities using Autosal readings. Measurement differences were within manufacturer specifications and small relative to in situ spatial changes. Standard manufacturer preprocessing routines were applied to the data. Other tests attributed flags to doubtful data of temperature, salinity, and pressure from the SBE37 based on expected ranges and visual inspection.

### 2.3. Turbulence Data

A series of 45 turbulence profiles were collected under the ice cover in Anse-Saint-Jean between 8 and 10 February 2011 using a loosely tethered coastal Vertical Microstructure Profiler (VMP-500) manufactured by Rockland Scientific International. This is the same profiler that Bourgault *et al.* [2012a] used 1 year earlier (on 11 February 2010) from which 15 profiles were collected at virtually the same site. Details about this instrument are presented in Bourgault *et al.* [2012a] and will therefore not be repeated here. For the purpose of this study and in order to increase statistical significance, the Bourgault *et al.* [2012a] data set (15 profiles) and the one collected later (45 profiles) were analyzed and interpreted together as a single data set, irrespective of the year they were collected in, with the hope that it could be considered as representative of winter conditions. From this combined data set, the mean diffusivity profile  $\bar{K}(z)$  was computed following the Osborn [1980] method, as well as the 95% confidence intervals using the bootstrap method with 500 replicates [Efron and Gong, 1983].

### 2.4. Environmental Parameters

Hourly water levels were obtained from a permanent tide gauge located at the end of the southern arm of the fjord, at Port Alfred (Fisheries and Oceans Canada, Canadian tides and water levels data archive) (Figure 1). Daily averages of wind magnitude and direction were provided by a meteorological station at Île Rouge (Environment Canada, climate—daily data report) (Figure 1). Daily average discharge data of the Saguenay River were provided by Rio Tinto Alcan (L. Salesse, personal communication, 2014) and monthly averages of the St. Lawrence discharge were obtained from Galbraith *et al.* [2015].

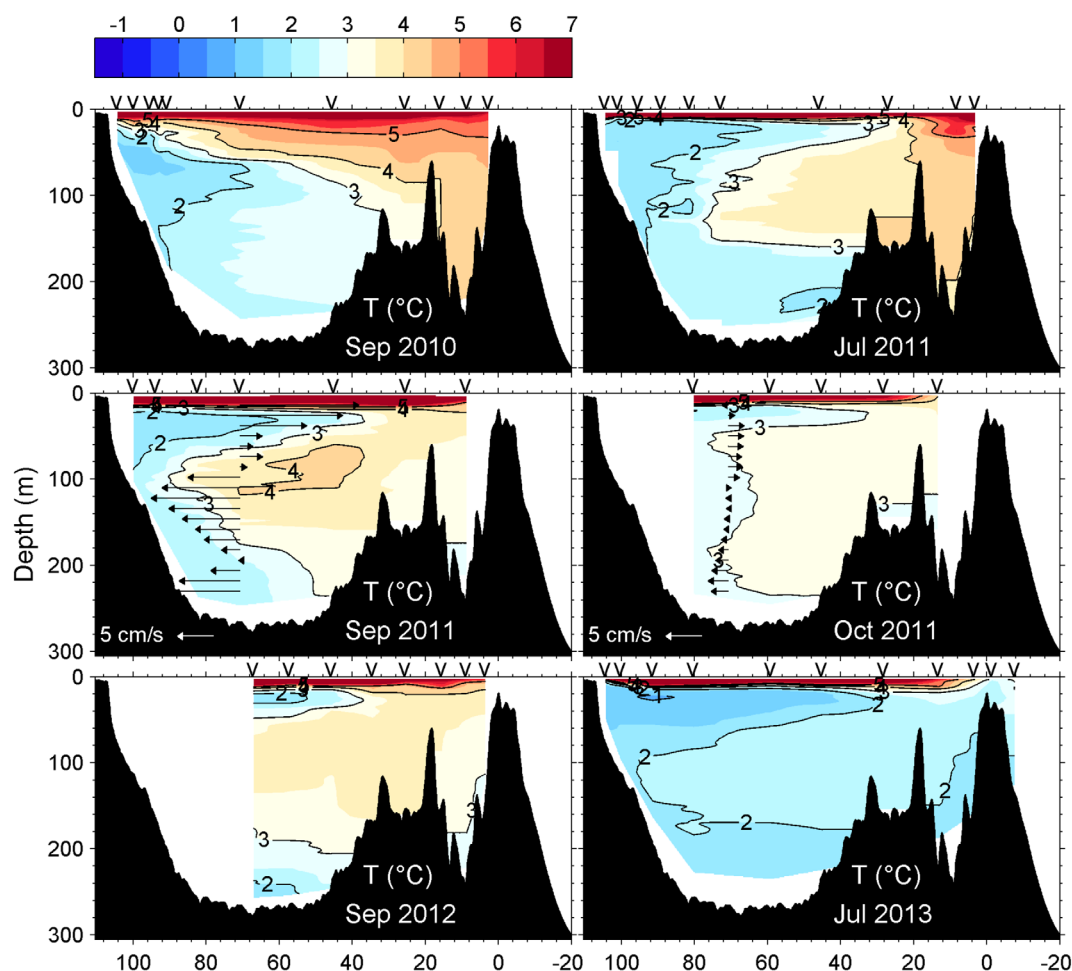


**Figure 2.** Observed temperature fields on 19–20 September 2010, 27 July 2011, 17–19 September 2011, 13 October 2011, 28 September 2012, and 23 July 2013. The fields were vertically smoothed over 5 m. Current vectors have been added to the September 2011 and October 2011 parts, showing residual filtered currents over 6 m (only one out of two vertical averages are illustrated on these panels). The V symbols on the top of the figures show the locations of the profiles.

### 2.5. Historical Observations

Archived data from two moored CTDs deployed by DFO on the fjord side of the mouth sill at 36 m depth in May 1998 and November 2002 are also used. A portion of the first record was published in *Bélanger* [2003].

## 3. Results

### 3.1. Hydrographic Observations

The water column circulation and T-S properties exhibit complex vertical structures evolving from monthly to seasonal timescales (Figures 2–5). While it is difficult to observe any patterns in the salinity fields of the inner basin other than the interannual variability (Figures 3 and 4), the temperature structure varies greatly over seasons with the surface layer being warm in summer ( $T \sim 10^\circ\text{C}$ ) and close to freezing point in winter (minimum observed of  $0^\circ\text{C}$ ) while the rest of the water column exhibits a more complex multilayer structure in the  $0\text{--}4^\circ\text{C}$  temperature range (Figures 2 and 4). The summer temperature fields (July–September) feature a relatively warm middepth SIW layer in every transect (Figure 2). This layer varied in thickness (from 120 to 200 m), in depth (centered from 100 to 160 m) and in temperature (max from 2 to  $4^\circ\text{C}$ ), showing large interannual and intraannual variability (Figure 2).

In September 2011, as it will be shown later in the mooring time series, the residual current velocities show fast intermediate and deep renewals occurring simultaneously ( $12$  and  $11\text{ cm s}^{-1}$ , respectively), both fast enough to be classified as strong renewal events ( $|u| > |\bar{u}| + 2\sigma \sim 5\text{ cm s}^{-1}$ , where  $u$  is the renewal event

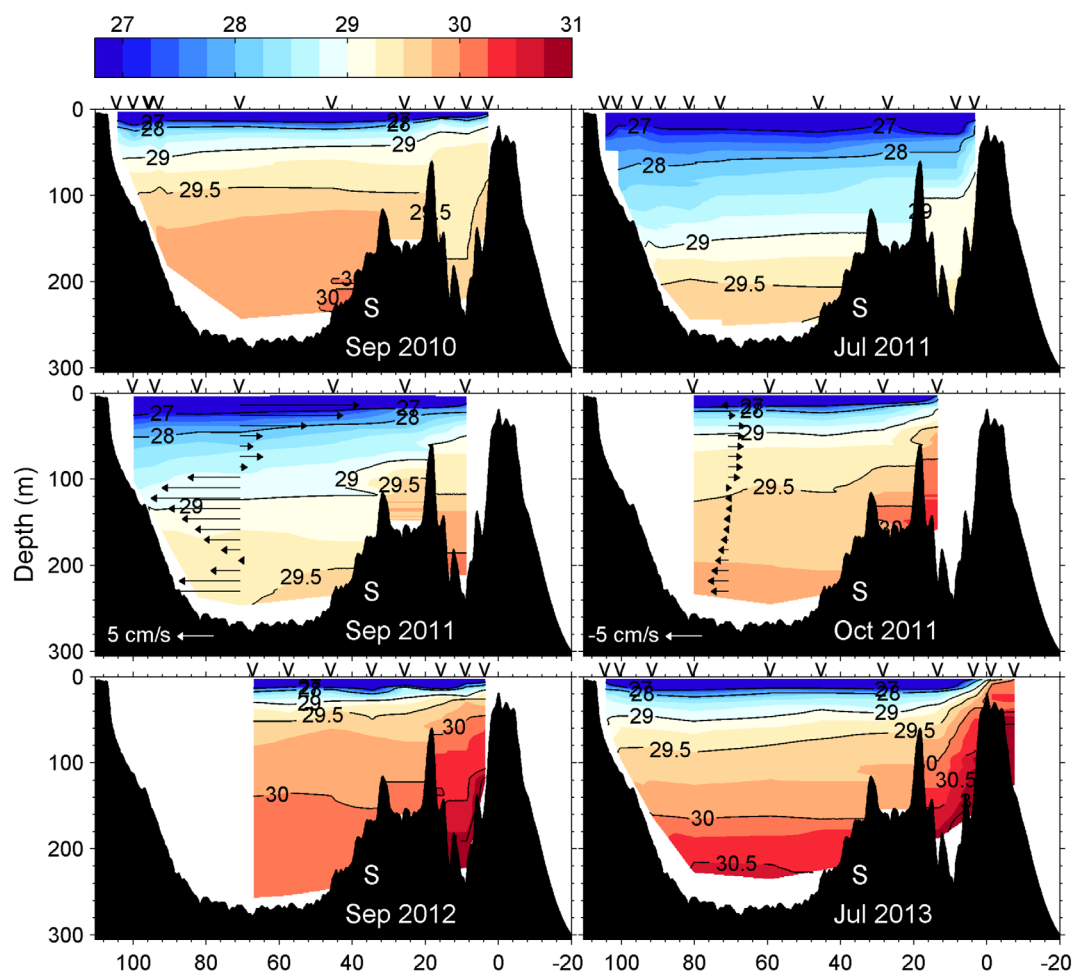


**Figure 3.** Observed salinity fields on 19–20 September 2010, 27 July 2011, 17–19 September 2011, 13 October 2011, 28 September 2012, and 23 July 2013. The fields were vertically smoothed over 5 m. Current vectors have been added to the September 2011 and October 2011 parts, showing residual filtered currents over 6 m (only one out of two vertical averages are illustrated on these parts). The V symbols on the top of the figures show the locations of the profiles.

velocity,  $\bar{u}$  the average inflowing velocity over the mooring period and over the total depth ( $\bar{u} = -1.67 \text{ cm s}^{-1}$ ), and  $\sigma$  the standard deviation ( $\sigma = 1.62 \text{ cm s}^{-1}$ ) (Figures 2 and 6, #2a and 1a).

In the winter season, one surprising observations is the clear occurrence of very cold shallow subsurface renewals (15–50 m depth) seen in March 2012 and 2013 (Figure 4). Such renewals have not been previously mentioned in the literature and we will refer to the water mass they bring as the Saguenay Shallow Water (SSW) ( $-1.5 < T < 1.0^\circ\text{C}$ ,  $27.0 < S < 29.5$ ). The density of this cold water is such that it spreads above the warmest waters found in the basin (Figure 4). In 2012, the subsurface intrusion was associated with  $6 \text{ cm s}^{-1}$  current velocities at the mooring position (Figures 4 and 6, #3b).

Evidences of previous or ongoing cold deep renewals are illustrated in the deepest part of the inner basin in March 2011 and 2012 (Figure 4). This water mass seems to correspond to what *Bourgault et al.* [2012a] called Saguenay Deep Water. Finally, the temperature fields of March 2011 and 2012 suggest deep renewals occurring in the outer basin (Figure 4). Indeed, because the outer basin was stratified in salinity (Figure 4), the homogeneous temperature in the outer basin cannot be explained by turbulences associated with sill processes and can only be the result of waters as cold as those intruding the subsurface, but denser, renewing the bottom of the outer basin.

In all three winter transects, a warm water mass ( $\sim 2.5^\circ\text{C}$ ) was found at the head of the fjord, from about 10 m depth to 50–75 m depth depending on the year (Figure 4). In summer, however, this pocket is

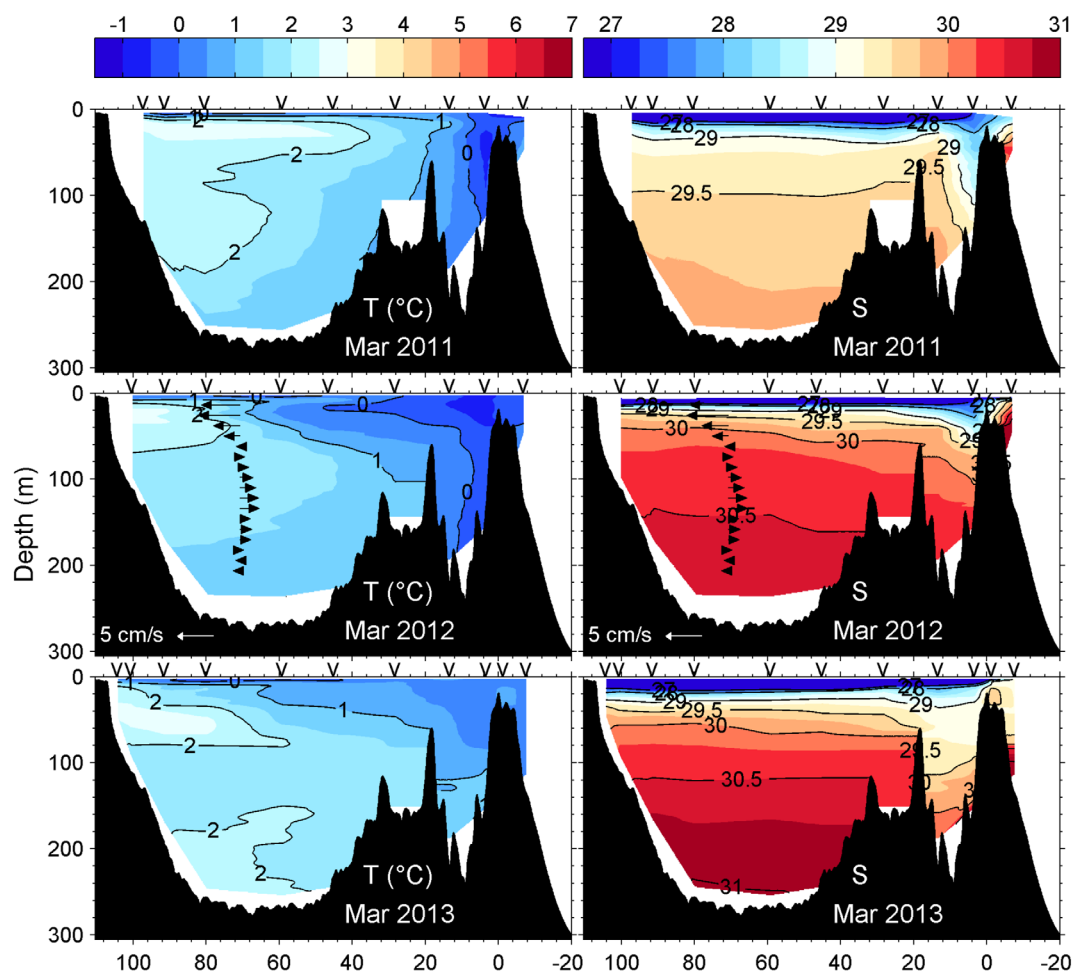


**Figure 4.** Observed (right) temperature fields and (left) salinity fields on 9 March 2011, 5 March 2012, and 5 March 2013. The fields were vertically smoothed over 5 m. Current vectors have been added to the March 2012 parts, showing residual filtered current over 6 m (only one out of two vertical averages are illustrated on this part). The V arrows on the top of the figures show the locations of the profiles.

occupied by the coldest waters within the fjord (Figure 2), which at  $\sim 1.5^\circ\text{C}$  are even colder than the  $2.5^\circ\text{C}$  temperature found in winter.

### 3.2. Mooring Observations

An unexpected feature is the important and sudden shift that occurred in the circulation regime in mid-February 2012 (Figure 6, #4). The shift was characterized by a change in the depth at which the overall renewal pattern occurred, thus implying that the salinity of the intrusions had changed. From the end of September to mid-February, the inflows from the St. Lawrence filled the bottom 150 m of the basin and the compensating return current flowed between 15 and 100 m depth. From 18 February to mid-July, the intrusions appeared mostly from the thermohalocline to about 90 m. The regime shift also coincides with a salinity decrease and a temperature increase below 75 m depth (Figures 5e and 5f).

From September 2011 to mid-February 2012, three strong renewal events ( $|u| > 5 \text{ cm s}^{-1}$ ) occurred in the deepest part of the inner basin (Figure 6, #1a–1c, inflow speed of  $\sim 11$ , 9, and  $7 \text{ cm s}^{-1}$ , respectively). The first one lasted at least 19 days, renewed the intermediate water as well (Figure 6, #2a) and brought in warmer ( $\Delta T = 0.6^\circ\text{C}$ ) and saltier ( $\Delta S = 0.6$ ) water (Figures 5e and 5f). The other two strong deep events lasted, respectively, 12 and 18 days and brought in colder ( $\Delta T = -0.4^\circ\text{C}$  and  $\Delta T = -0.6^\circ\text{C}$ , respectively) and saltier ( $\Delta S = 0.3$  and  $\Delta S = 0.4$ ) water (Figures 5e and 5f). Furthermore, the isotherms and isohalines of Figure 5 show that the three deep water renewals affected nearly the entire water column (up to 50 m depth). Within 2–4 weeks, it is likely that the resident water was uplifted by the denser deep renewals until it reached the return current to find its way out. For example, the water mass that renewed the bottom of the

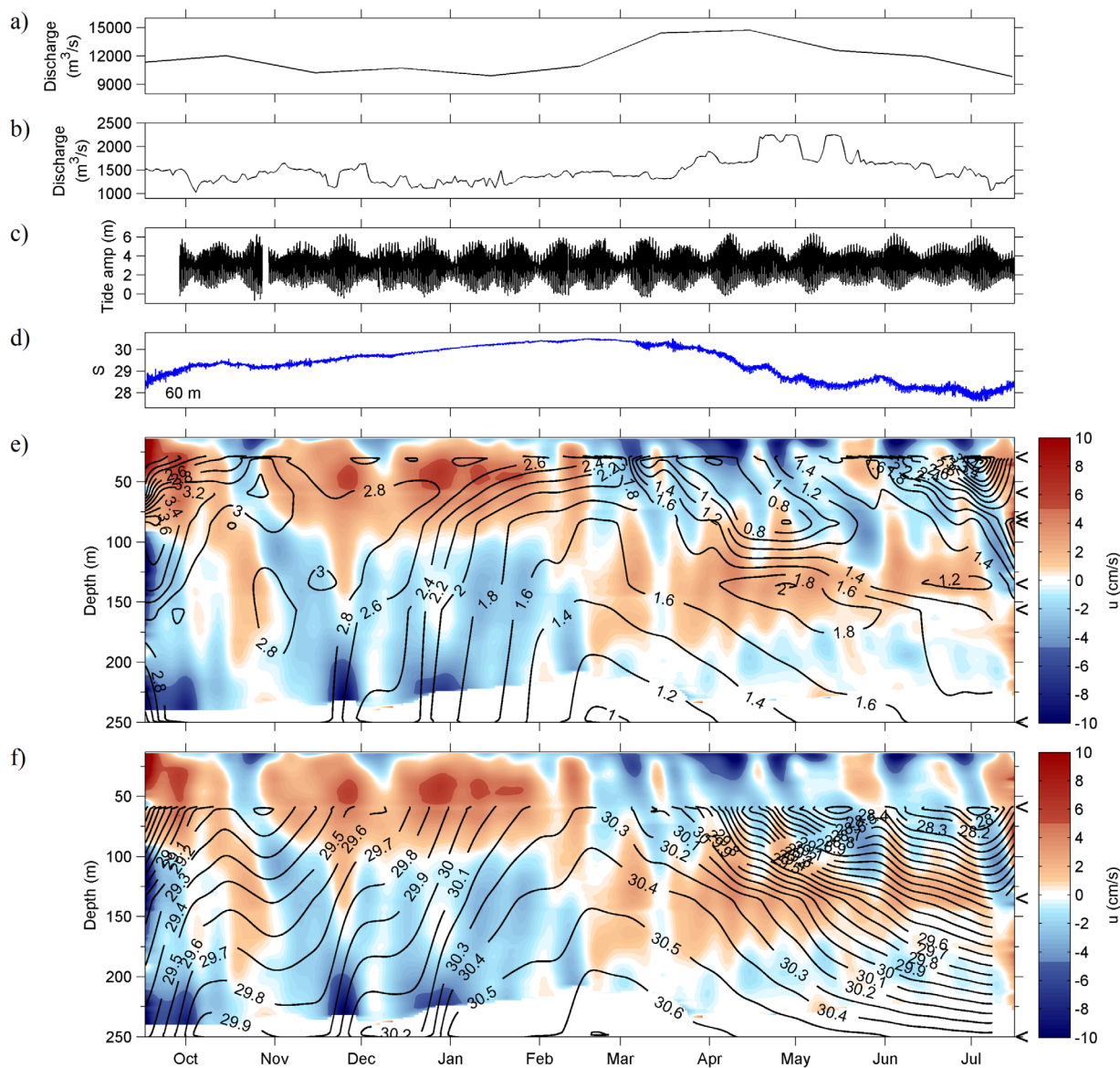


**Figure 5.** Mooring B1 observations and associated environmental parameters in 2011–2012. (a) Monthly St. Lawrence River discharge. (b) Daily Saguenay River discharge. (c) Hourly tidal water level at Port Alfred. (d) Observed salinity at 60 m depth at the mooring position. (e) Time series of the low-pass filtered along-shore currents ( $u$ ), at B1, superimposed by filtered isotherms. Positive currents correspond to downstream flow, or outflow. There are jumps into the color map to highlight the strong renewal velocities lower than  $-5 \text{ cm s}^{-1}$  or the return currents greater than  $5 \text{ cm s}^{-1}$ . Time series of the same along-shore currents ( $u$ ) superimposed by filtered isohalines (f). The arrow symbols on the right-hand side are the locations of the instruments providing temperature and salinity.

inner basin in late November (Figure 6, #1b) was a water mass characterized by a temperature of  $2.5\text{--}2.9^\circ\text{C}$  and a salinity of  $29.9\text{--}30.1$  (Figures 5e and 5f). The same T-S properties were seen about 4 weeks later flowing outward at 75 m depth (Figures 5 and 6, #5a). During the three deep water renewal events, the return current appeared to be stronger and thicker (Figure 6).

Additionally, six strong shallow subsurface renewal events, just underneath the pycnocline, were seen during the sampling period. One occurred in late October 2011 (Figure 6, #3a, inflow speed of  $\sim 7.5 \text{ cm s}^{-1}$ ) and the others occurred from March to July 2012 (Figure 6, #3b–3f, inflow speed of  $\sim 6.0, 10.5, 9.0, 11.0,$  and  $8.5 \text{ cm s}^{-1}$ , respectively). The subsurface renewal that occurred in March 2012 (Figure 6, #3b) is also seen in the hydrographic transect (Figure 4). In the same way that the isotherms and isohalines show the displacement of water associated with deep renewals, they also show that the subsurface renewals have displaced the resident water downward, replacing the first 100 m of the water column (Figure 6, #6a–6c).

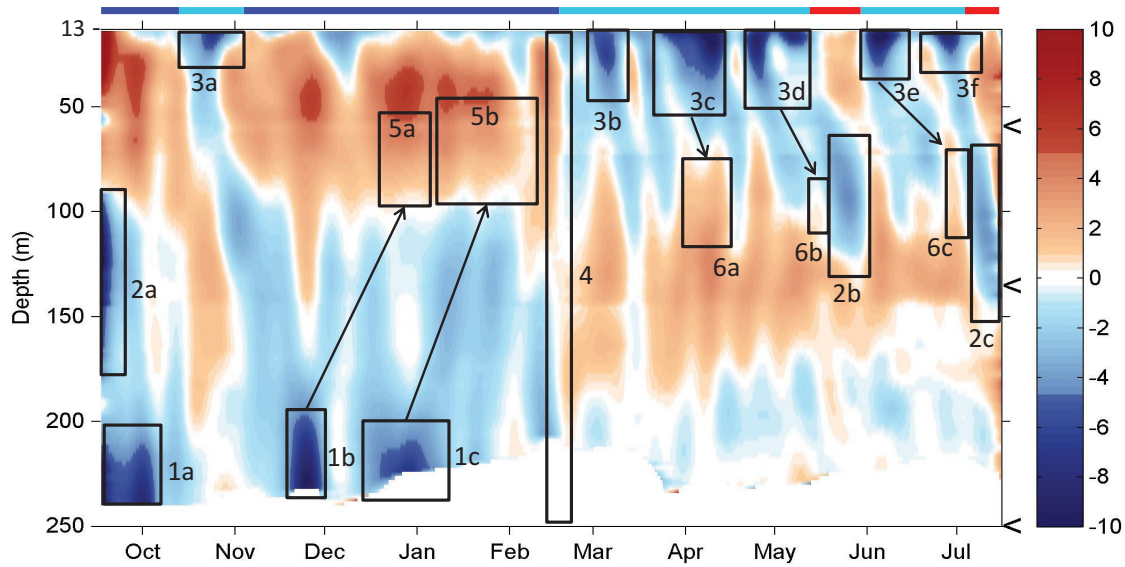


**Figure 6.** Same as the two bottom parts of Figure 5, low-pass filtered along-shore currents at B1, to better highlight some circulation features discussed in the text (outward currents are positive). The colored line segments at the top correspond to the periods where the three types of renewal occurred (the colors coincide with the colors in Figure 7).

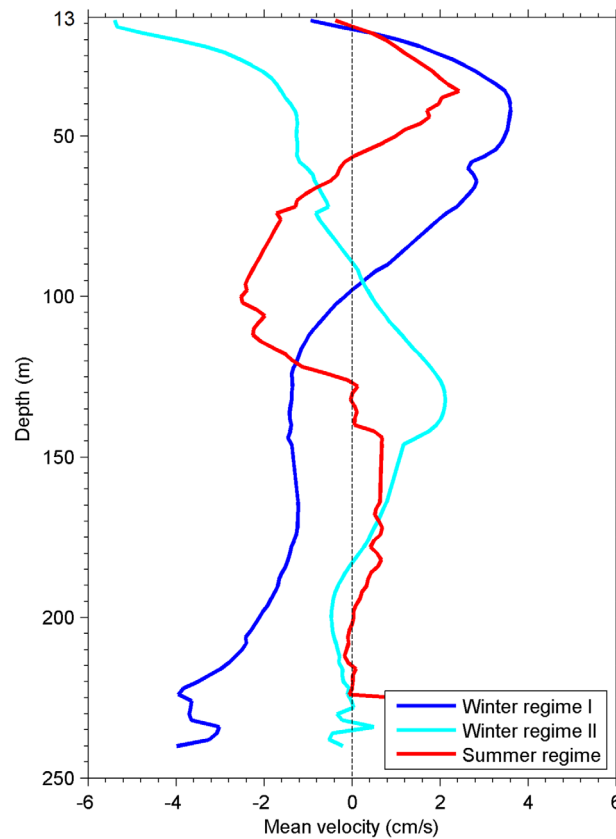


**Figure 7.** Velocities averaged over periods relative to the three renewal types. The averaging periods are indicated by color-coded line segments in Figure 6.

Finally, three renewal events occurred at intermediate depths (between 60 and 175 m depth) in late September, in late May and in July (Figure 6, #2a–2c). Only the September event is considered a strong event (velocity of  $\sim 12 \text{ cm s}^{-1}$ ). When intermediate events occurred, return currents were formed above the inflows.

The three different intrusion types are illustrated in Figure 7, each curve corresponding to an average of the velocities over the periods they occurred. The winter regime I corresponds to deep renewals (SDW), winter regime II to subsurface ones (SSW), and summer regime to intermediate renewals (SIW).

A typical renewal event can travel through the entire inner basin in less than 2 weeks while displacing the resident water toward the return current, renewing part of the inner basin. Based on the isotherms and isohalines, this displacement process could take an additional 2–4 weeks depending on the speed of the inflows (e.g., from box 1b to 5a, 1c to 5b, 3c to 6a, 3d to 6b, and 3e to 6c in Figure 6). The deep events have the potential to fully renew the inner basin in about 1–1.5

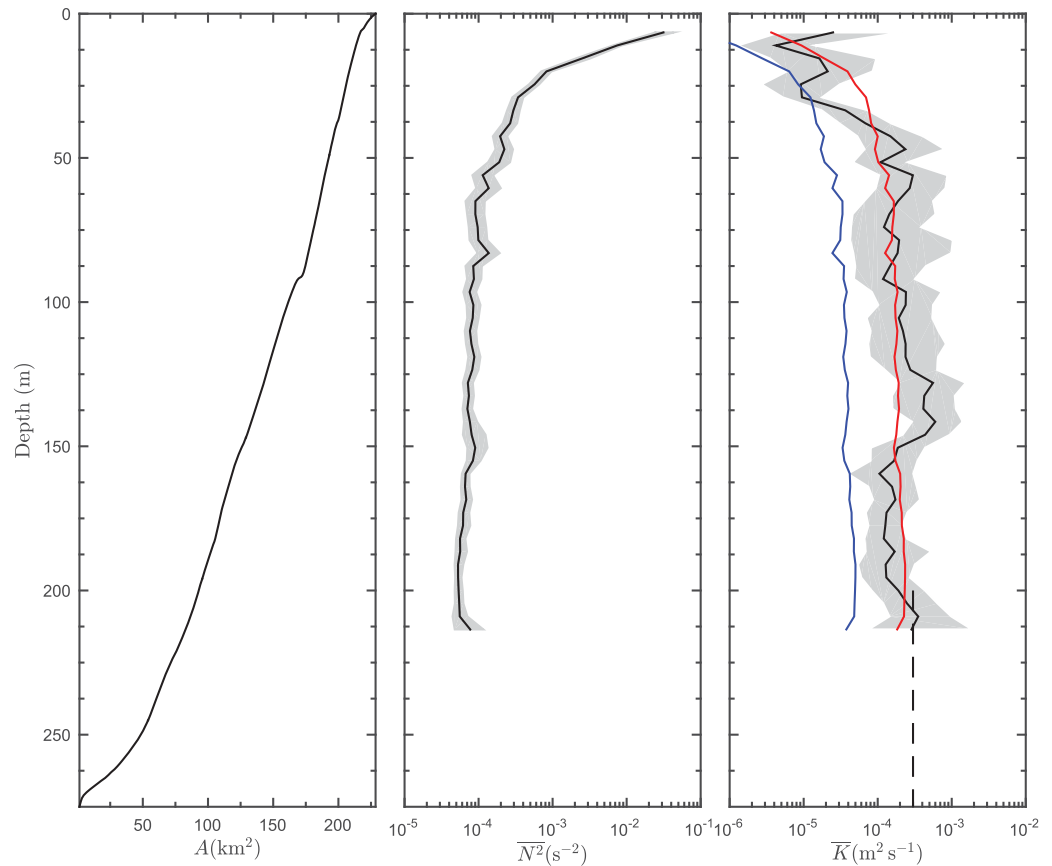


**Figure 8.** Profiles of (left) horizontal cross-section area  $A$  of the inner basin, (middle) mean buoyancy frequency squared  $\overline{N^2}$ , and (right) mean diffusivity  $\overline{K}$ . In the middle and right parts, the solid and shaded curves represent, respectively, the mean and 95% bootstrapped confidence intervals computed from 60 turbulence profiles collected in Anse-Saint-Jean from ice camps in February 2010 and 2011. The dashed line represents the diffusivity inferred from the budget method ( $K_b \sim 3 \times 10^{-4} \text{ m}^2 \text{ s}^{-1}$ ) as detailed in the text. The blue curve represents the parameterization used in the model of *Stacey and Gratton* [2001] for fixing the minimum diffusivity  $K_{V\min}$  as function of  $N^{-1.5}$  and the red curve is a least squares fit of the power law  $\overline{K} = a(\overline{N}/N_0)^b$  with  $a = 3.8 \times 10^{-7} \text{ m}^2 \text{ s}^{-1}$  and  $b = -1.3$  (see text for more details and uncertainties).

months at the mooring position. The isotherms and isohalines show that the inner basin was renewed entirely 3 times in fall and early winter 2012 but not the rest of the year (Figures 5e and 5f). In spring, the bottom part of the basin shows a decrease in salinity (Figure 5f), implying that vertical diffusive processes were active and that the deep water was not renewed until at least the end of the following summer (6 months later). Stratification also increases during the summer in the bottom layer. The subsurface events would only renew the water on the top 100 m of the water column and depending on the strength of the event, the intermediate events can renew almost the entire basin except for the denser water found at the bottom.

### 3.3. Turbulence Observations

Analysis of all combined turbulence profiles indicates that the top part of the water column ( $< 30 \text{ m}$ ) is characterized with much lower diffusivity ( $\overline{K} \sim 10^{-5} \text{ m}^2 \text{ s}^{-1}$ ) than the deeper ( $\geq 50 \text{ m}$ ) layers ( $\overline{K} \sim 10^{-4}$  to  $10^{-3} \text{ m}^2 \text{ s}^{-1}$ ) during winter (Figure 8, right). The deep depth-averaged diffusivity, below 50 m, is  $\overline{K}_{\text{deep}} = 2 \times 10^{-4} \text{ m}^2 \text{ s}^{-1}$ . Note that with only 60 profiles available, the uncertainty is large (roughly an order of magnitude). An independent estimate of the horizontally averaged values of the vertical eddy diffusivity ( $K_b$ ) was then calculated using the budget method [Stigebrandt and Aure, 1989; Stigebrandt, 2012],

$$K_b = \frac{1}{A_0 \frac{\partial S}{\partial z}} \int_{-H}^{z_0} \frac{\partial S}{\partial t} A \, dz, \quad (1)$$

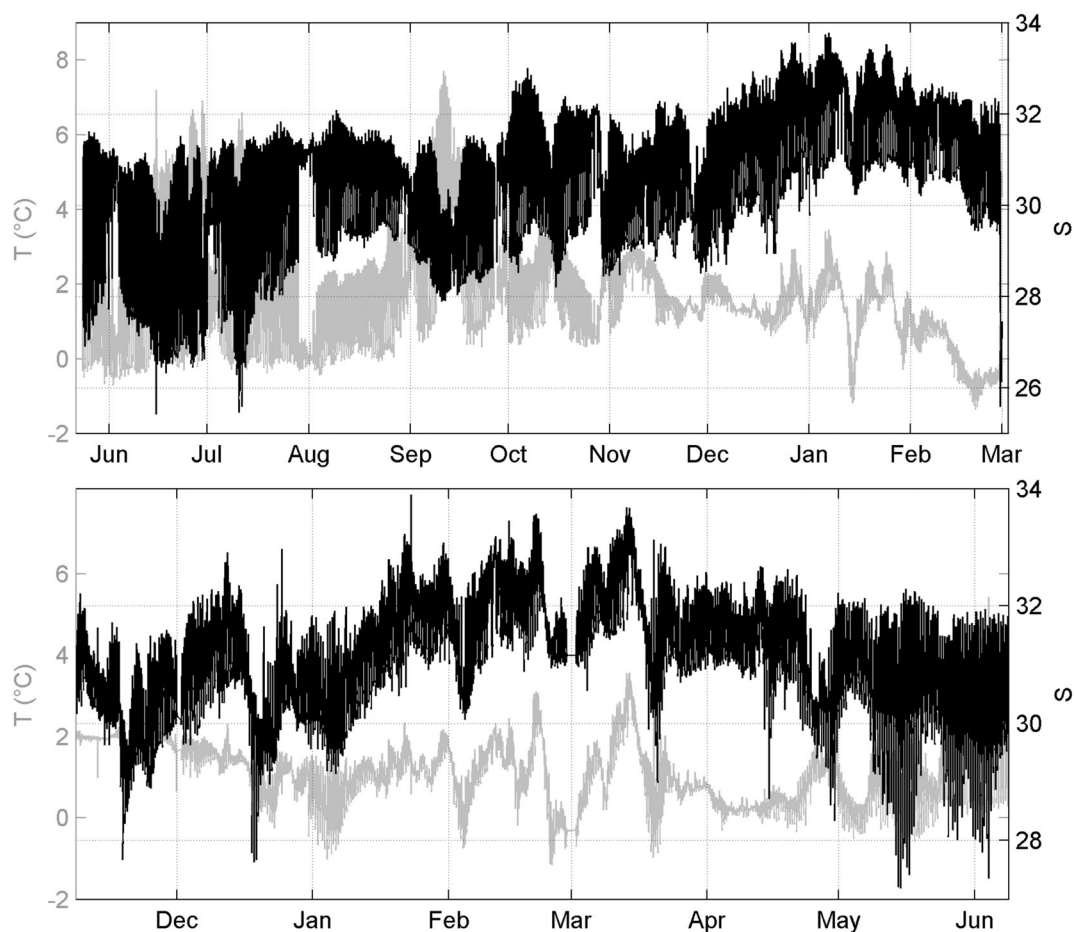


**Figure 9.** Temperature (grey) and salinity (black) time series of moored CTDs on the sill at the fjord entrance at 36 m depth (top) in 1998–1999 and (bottom) in 2002–2003.

where  $H$  is the total depth,  $z_0$  is a reference level,  $A$  is the horizontal cross-section area at depth  $z$  and  $A_0$  the area at depth  $z_0$  both following the hypsographic function of the inner basin shown in Figure 8,  $\frac{\partial S}{\partial z}$  was approximated by taking the salinity difference between measurements at depth  $z_0$  and  $H$  from a profile in the inner basin of the Saguenay in March 2011, and  $\frac{\partial S}{\partial t}$  was approximated by taking the salinity difference between measurements in March and July 2011 at depth  $z$ . This method can only be used in period of stagnation as it excludes advection fluxes. As the Saguenay is never stagnant over the entire water column, the calculation was made below the middepth density-driven inflow (i.e.,  $z_0 \leq -200$  m) between hydrographic observations of March 2011 and July 2011, yielding a depth-averaged value of  $\bar{K}_b \sim 3 \times 10^{-4} \text{ m}^2 \text{ s}^{-1}$  for all depths below 200 m (Figure 8). The implication of these results for deep water renewals will be further discussed in section 4.3.

## 4. Discussion

### 4.1. Circulation Dynamics and Renewal Time

As observed in all our transects, the summertime water temperatures are lowest, while the wintertime water temperatures are highest, in a pocket located at the head of the fjord just underneath the main pycnocline and down to about 100 m (Figures 2 and 4). Because summer temperature minima are always lower than the winter maxima, it is deduced that this pocket of water does not contain the same water mass all year round. Our interpretation is that the cold pocket of water found there in summer corresponds to the cold subsurface water (SSW) of the previous winter, trapped by new input of intermediate water (SIW). There is no indication that this pocket of water resulted from deep water displaced upward, because at mooring B1, during the uplift-favorable period prior to mid-February, waters colder than 1.5°C were only observed

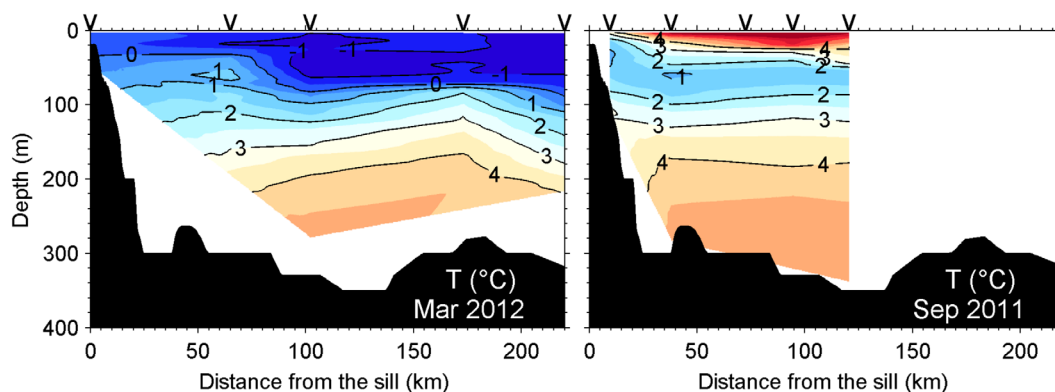


**Figure 10.** Temperature field of the St. Lawrence Estuary during (left) 5–6 March 2012 and (right) 20–24 September 2011. The V arrows on the top of the figures show the locations of the profiles.

during a brief period up to 150 m depth and could not have been uplifted to 75 m before the mid-February regime shift (Figure 5e). However, in winter, this region of the fjord is actually occupied by water showing a maximum of temperature and, as presented by *Bourgault et al.* [2012a], it is probably the SIW residual formed during summer, eroded over fall and winter and displaced upward by the arrival of denser deep water. Because there are indications that this pocket of water corresponds to water from previous seasons, the estimated renewal time of the region would be a maximum of 6 months as it would be renewed at least twice a year. *Loucks and Smith-Sinclair* [1975] estimated an inner basin residence time of 2–6 months. This time scale is consistent with our observations that imply a renewal time at the mooring position of between 1 and 6 months.

One new result is the sudden seasonal shift in the circulation regime observed in mid-February, accompanied by a change in the temperature and salinity trends (Figures 5e and 5f). We suggest that this regime shift is controlled by the seasonal cycle of salinity of the St. Lawrence Estuary waters present near the fjord entrance sill, which dictates the intrusion depths into the fjord. Unfortunately, there are no observation available at the sill during our sampling period, but two temporal T-S series were collected on the sill in 1998–1999 and in 2002–2003 (Figures 1 and 9). The salinity at the sill increased continually during fall until it reached a maximum sometime in winter. The water mass properties associated with these maximums found in January 1999 ( $T = 3.48^{\circ}\text{C}$  and  $S = 33.8$ , Figure 9) and in February and March 2003 ( $T = 3.58^{\circ}\text{C}$  and  $S = 33.67$ , Figure 9) are characteristic of Gulf of St. Lawrence deep waters advected into the Gulf from the continental slope. Indeed, water with the same T-S properties was found in the Gulf of St. Lawrence, or in the Estuary, in March of the respective years at 175 and 116 m depth, respectively (DFO T-S profiles from the March helicopter-based survey).

The mechanism behind the salinity seasonal cycle of the St. Lawrence could be related to the low-frequency modulation of the St. Lawrence estuarine circulation. In autumn and early winter, the CIL is eroded and mixed with the surface layer leading to a two-layer estuarine circulation (Figure 10, left) rather than in a three-layer circulation that characterizes summer conditions (Figure 10, right) [*Saucier et al.*, 2009]. As strong westerly wind forcing pushes the Estuary surface layer toward the Gulf, it promotes, by continuity, the inland advection of deep, salty and relatively warm waters [*Smith et al.*, 2006]. Deep isotherms and isohalines would then rise in the Estuary, and deeper denser waters become available for fjord renewals, promoting deep inner basin renewals.

In winter or early spring, when the advection of the Gulf surface mixed layer intensifies toward the head of the Estuary (as seen as a cold intermediate layer at 100 km from the sill in Figure 10, left), the upstream estuarine circulation decreases in the deep layer and increases in the intermediate layer [*Smith et al.*, 2006; *Saucier et al.*, 2009]. The isohalines then sink and the water present at the fjord sill becomes fresher and colder (Figure 9). A T-S diagram from February 1999 shows that the coldest waters present at the sill had the lowest densities (Figure 11). These could explain subsurface renewals observed from the circulation shift until summer.

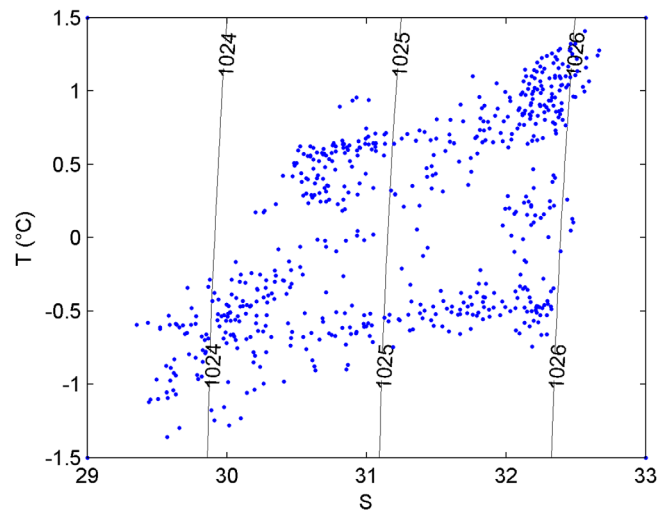


**Figure 11.** T-S diagram of a CTD moored on the shallowest sill at 36 m depth during February 1999 [Bélanger, 2003]. The contour lines are isopycnals.

There is a high interannual variability in the salinity seasonal cycle of water present at the sill. In 1999, the maximum salinity occurred in early January, while in 2003 it occurred in March (discounting a brief spike in late January) (Figure 9). The variability of winter water masses in proximity to the sill at depths shallower than 100 m is also documented by the March helicopter-based survey. Between 2000 and 2013, the Gulf of St. Lawrence winter mixed layer water ( $T < -1^{\circ}\text{C}$ ,  $S > 32$ ) was observed to have reached the area of the sill once, in 2004 (red rectangle in Figure 12), meaning that the shift of the St. Lawrence circulation had already occurred before March of that year. In other years, deep estuarine waters ( $T > 2^{\circ}\text{C}$ ,  $S > 33$ ) were observed twice at shallow depths (16–56 m), in 2003 and 2007 (black rectangle in Figure 12), which suggests that the shift then occurred later than March.

Shorter time scale salinity variations also occurred throughout the mooring record (Figure 5d). Changes in the sign of the temporal salinity gradient coincide with changes in the intrusion depth in the inner basin whereby increasing salinity coincides with later deeper intrusions (Figures 5d and 5f). For example, the two middepth renewals of May and July (Figure 6, #2b and 2c) were associated with an increase in salinity, while the isolated subsurface renewal of October (Figure 6, #3a) was associated with a decrease in salinity (Figure 5f). On even smaller time scales, the salinity of the waters present at the sill can vary by 2–4 within a single semidiurnal cycle, with maximum salinity and maximum temperature present around high tide (Figure 9).

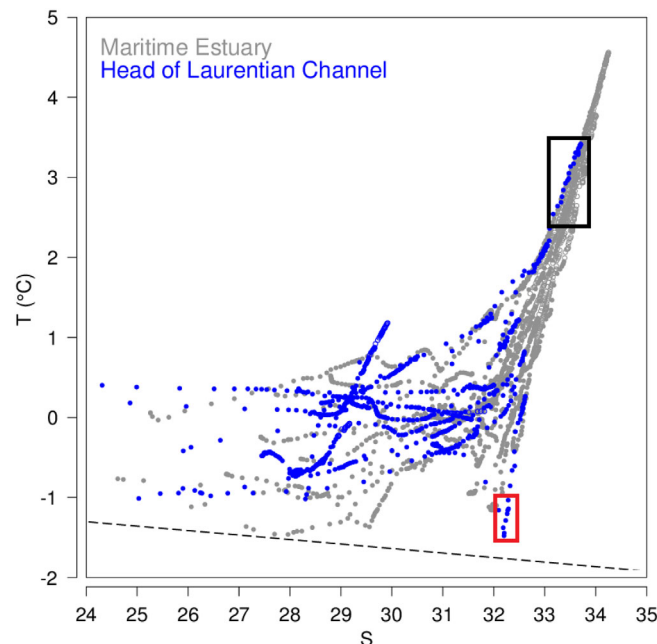


**Figure 12.** T-S of CTD casts made in the Estuary (grey dots) and near the sill (blue dots) during March helicopter-based survey from 2000 to 2013. The red rectangle highlights observations characteristic of the Gulf of St. Lawrence winter mixed layer water and the black rectangle highlights observations characteristic of typical deep estuarine water.

The salinity difference between tidal phases is sufficient to considerably change the depth of intrusions. This high salinity variation may explain why both subsurface and deep cold water renewals were observed in March 2012 and 2013 in the outer basin (Figure 4).

The salinity difference between tidal phases is sufficient to considerably change the depth of intrusions. This high salinity variation may explain why both subsurface and deep cold water renewals were observed in March 2012 and 2013 in the outer basin (Figure 4).

The salinity difference between tidal phases is sufficient to considerably change the depth of intrusions. This high salinity variation may explain why both subsurface and deep cold water renewals were observed in March 2012 and 2013 in the outer basin (Figure 4).

The salinity difference between tidal phases is sufficient to considerably change the depth of intrusions. This high salinity variation may explain why both subsurface and deep cold water renewals were observed in March 2012 and 2013 in the outer basin (Figure 4).

#### 4.2. Environmental Factors

Bélanger [2003] suggested there was a connection between episodes of north-east wind and the absence of deep summer renewals in the inner basin. Unfortunately, there were no current and density observations directly at the sill during the mooring period to investigate if such a correlation could be detected with wind observations at Île Rouge (wind observations not shown). The mooring was 70 km away from the sill and the distance introduces important time lags between the advection over the sill and the readings at the mooring position. Furthermore, the period when

the correlation was observed by *Bélanger* [2003], August, was not recorded in our time series. Therefore, the present data set does not allow to test the wind hypothesis of *Bélanger* [2003].

There are slight indications that occurrences of the strong renewal events, seen in fall and winter, are controlled by the neap-spring and monthly tidal modulation, which would be consistent with the findings of *Bélanger* [2003]. The periods between the beginnings of two consecutive strong events (29.7 and 30.4 days) roughly correspond to two fortnightly cycles (Figures 5c and 5e). In Puget Sound, Washington, deep renewals are associated with neap tides as the turbulence at the sill is too strong during spring tides to permit dense renewals [*Geyer and Cannon*, 1982]. It is difficult to know if it is the case in the Saguenay as, once again, there are no observations directly at the sill. During spring and summer, in the Saguenay, the timings of consecutive renewal events were irregularly spaced (21.6, 29.7, 40.2, and 22.6 days) and no controlling factors, in terms of renewal event frequency, have been identified for this period.

The monthly St. Lawrence runoff may also have an impact on renewal depths. For example, the runoff was slightly higher in October 2011 ( $12,000 \text{ m}^3 \text{ s}^{-1}$ ) than in September and November of the same year (11,300 and  $10,200 \text{ m}^3 \text{ s}^{-1}$ , respectively) (Figure 5a). This may have lowered the inflowing water density and induced the shallower renewal observed in October (Figure 6, #3a). The interpretation of the St. Lawrence discharge influence has to be taken lightly as the monthly averages hide higher frequency variations. The Saguenay runoff variation does not seem to explain any variations in the fjord circulation (Figure 5b).

### 4.3. Turbulent Mixing

Although the turbulence measurements presented in Figure 8 are rather sparse and the budget method calculations were not made during a stagnation period for the entire water column, several remarks are worth mentioning regarding the role that turbulent mixing may play for deep water renewals. Our year-long moored observations, multiseasons CTD transects and observations of well-oxygenated deep waters [*Drainville*, 1968; *Taylor*, 1975; *Therriault and Lacroix*, 1975] indicate that major replacements of deep water occur on at least an annual basis. As mentioned earlier, a summer or fall deep renewal event can really only occur if the deep water mass from the previous winter has had its density sufficiently lowered by vertical mixing to allow new dense water to intrude underneath. In the Saguenay, the deep diffusivity ( $\geq 50 \text{ m}$ ) ( $\sim 10^{-4} \text{ m}^2 \text{ s}^{-1}$ ) is quite large especially as the measurement took place away from the sills and seabed (i.e., not driven by boundary mixing) (Figure 8). It is higher by about an order of magnitude than in the adjacent St. Lawrence Estuary at comparable depths [*Cyr et al.*, 2011; *Bourgault et al.*, 2012b].

These remarks naturally raise the question about the cause of such large deep turbulent mixing in the Saguenay Fjord. The presence of sea ice in winter, hindering wind-induced mixing, excludes the atmosphere as a turbulence source in February and may explain why the deep diffusivity is larger than in the surface layer (Figure 8). The tides are often the main source of energy for mixing and circulation in basin waters [*Gade and Edwards*, 1980]. The tidal energy can be extracted as friction against boundaries, baroclinic wave drag, tidal jets, and high-frequency internal waves [*Fer and Widell*, 2007]. Based on the *Stigebrandt and Aure* [1989] method, the densimetric Froude number ( $F_d$ ) can be used to theoretically differentiate fjords that have internal wave generation ( $F_d < 1$ ) from the ones generating tidal jets ( $F_d > 1$ ),

$$F_d = \frac{\alpha H_b}{c_i H_t}, \quad (2)$$

where  $\alpha$  is the amplitude of the tidal speed defined as  $\alpha = a_f \omega \frac{A_f}{B_m (H_t + H_b)}$ , where  $a_f$  is the tide amplitude,  $\omega$  the frequency,  $A_f$  the horizontal surface area of the fjord,  $B_m$  the width of the mouth,  $H_t$  the sill depth, and  $H_b$  the basin depth (from sill depth to basin depth).  $c_i$  is the internal wave speed in a two-layer system defined as  $c_i = \sqrt{g \frac{\Delta\rho}{\rho_0} \frac{H_t H_b}{H_t + H_b}}$ , where  $g$  is the acceleration of gravity,  $\Delta\rho$  the difference between density below and above sill depth, and  $\rho_0$  the reference density. All numbers used in this calculation are listed in Table 2. The Saguenay Fjord is in supercritical (jet-type) condition at its first shallow sill through all of the tidal cycle with  $F_d \sim 13$ . The barotropic flow speed over the sill is then greater than the phase speed of internal tides in the basin. The sill area is characterized by strong turbulence and internal waves should not be able to propagate in the basin [*Stigebrandt*, 1976]. In order to compare with other fjords, the total energy flux across the entrance sill (56 MW from the simulations of *Stacey and Gratton* [2001]) is normalized by the horizontal surface area of the fjord at sill depth ( $A_t$  in Table 2) which gives  $\sim 220 \text{ mW m}^{-2}$ . This result is

**Table 2.** Topographical and Physical Information on Two Different Locations in the Saguenay Fjord, the Mouth Sill, and the Inner Sill

Location	$H_r$ (m)	$H_b$ (m)	$A_r$ (km <sup>2</sup> )	$A_i$ (km <sup>2</sup> )	$B_m$ (m)	$\rho_0$ (kg m <sup>-3</sup> )	$\omega$ (s <sup>-1</sup> )	$a_r$ (m)	$g$ (m s <sup>-2</sup> )	$\Delta\rho$ (kg m <sup>-3</sup> )
Mouth sill	18	252	265	250	1100	1024	$1.4 \times 10^{-4}$	3	9.81	1
Inner sill	115	155	220	150	1700	1024	$1.4 \times 10^{-4}$	3	9.81	0.5

much greater than the energy flux per surface area found in other jet fjords in Norway (1–142 mW m<sup>-2</sup>) [Stigebrandt and Aure, 1989; Stigebrandt, 2012]. This differentiates the Saguenay Fjord from those that connect directly to the coastal ocean, as the large tides in the Estuary are driving the jet conditions observed over the first sill. However, the jet is primarily an energy source of near-sill mixing [Inall and Gillibrand, 2010] and would contribute mostly to mixing in the outer basin. The dynamics of the inner basin are very different and less energetic. By considering the inner basin as an independent system, we get  $F_d \sim 0.5$  over the inner sill (115 m depth), meaning that internal waves may be generated and that part of the energy may be transferred to the inner basin water, contributing to the large vertical mixing.

#### 4.3.1. Internal Wave Mixing

Under the assumption that breaking internal waves provide the main source of turbulence within the lower layers of sill fjords [Stigebrandt, 1976], it has been argued that turbulent diffusivity could be parameterized as being inversely proportional to some power of the buoyancy frequency [Gargett and Holloway, 1984; de Young and Pond, 1988; Stigebrandt and Aure, 1989], that is,

$$K = a \left( \frac{N}{N_0} \right)^b, \quad (3)$$

where  $a$  is a constant of proportionality, which may differ from one fjord to another, and  $N_0 = 1 \text{ s}^{-1}$  is introduced here simply for scaling purposes such that the units of  $a$  (here in  $\text{m}^2 \text{s}^{-1}$ ) do not depend on the choice of the exponent  $b$ . Values for  $b$  are found in the literature to lie somewhere between  $-2.0 \leq b \leq -1.0$  [de Young and Pond, 1988; Stigebrandt and Aure, 1989; Stigebrandt and Kalén, 2013].

In their laterally integrated model of the Saguenay Fjord, Stacey and Gratton [2001] used a parameterization of turbulent diffusion based on the Mellor and Yamada [1982] level 2.5 turbulence closure scheme. However, and as discussed in greater details in Stacey et al. [1995], they further complemented their turbulence model with the parameterization above (equation (3)) in order to fix a lower bound on turbulent diffusivity. This lower bound is assumed to be the minimum background diffusion caused by unresolved breaking internal waves. Such processes are not taken into account in the Mellor-Yamada formulation. Accordingly, Stacey and Gratton [2001], as in Stacey et al. [1995], set the minimum diffusivity to

$$K_{Vmin} = a \left( \frac{N}{N_0} \right)^b, \quad (4)$$

with  $a = 3.1 \times 10^{-8} \text{ m}^2 \text{ s}^{-1}$  and  $b = -1.5$ .

The result of this parameterization is shown as the blue curve in Figure 8. Qualitatively, the comparison with the measurements suggests that the  $K \propto N^{-1.5}$  dependency adopted by Stacey and Gratton [2001] may be appropriate although this parameterization alone, with their chosen value for  $a$ , underestimates the observed deep diffusivity by roughly an order of magnitude. However, it must be kept in mind that Stacey and Gratton [2001] used this parameterization only as a lower bound and, as such, there is no indication here that this may not be appropriate. A more meaningful comparison would have been to compare the measurements with the total modeled diffusivity, i.e., the sum of the Mellor-Yamada contribution and the internal wave parameterization, but this information is not provided in Stacey and Gratton [2001].

A least squares fit of equation (3) to our measurements of  $\bar{N}^2$  and  $\bar{K}$  gives a significant correlation with  $R = 0.5$  ( $p \ll 0.01$ ) with the following parameters:  $a = 3.8 \times 10^{-7}$  ( $6.2 \times 10^{-9}$ ,  $3.6 \times 10^{-6}$ )  $\text{m}^2 \text{ s}^{-1}$  and  $b = -1.3$  ( $-2.2$ ,  $-0.8$ ), where the numbers in parentheses give the lower and upper bound of the 95% confidence interval on the fitted parameters. This relationship is shown as the red curve in Figure 8. This  $K \propto N^{-1.3}$  dependency determined here from direct turbulence measurements is consistent with values reported in the literature that have been determined indirectly from analyses of salinity and temperature fields [de Young and Pond, 1988; Stigebrandt and Aure, 1989]. Considering that this sort of dependency has

**Table 3.** Some Published Deep Basin Water Vertical Eddy Diffusivities, From the Less Turbulent to the Most Turbulent<sup>a</sup>

Location	$K_z$ (m <sup>2</sup> s <sup>-1</sup> )	Reference
Byfjorden, Sweden	$5 \times 10^{-7}$ to $6 \times 10^{-6}$	<i>Svensson</i> [1980]
7 Canadian fjords	$8 \times 10^{-6}$ to $9 \times 10^{-4}$	<i>Smethie</i> [1980]
St. Lawrence Estuary, Canada	$4 \times 10^{-5}$	<i>Cyr et al.</i> [2011]
Clyde Sea, Scotland	$5 \times 10^{-5}$	<i>Inall and Rippeth</i> [2002]
Gullmar Fjord, Sweden	$10^{-5}$ to $10^{-4}$	<i>Arneborg et al.</i> [2004b]
Storfjorden, Svalbard	$10^{-4}$	<i>Fer</i> [2006]
Saguenay Fjord, Canada	$2 \times 10^{-4}$	
VanMijenfjorden, Svalbard	$7 \times 10^{-4}$	<i>Fer and Widell</i> [2007]
Puget Sound, USA	$2 \times 10^{-4}$ to $7 \times 10^{-3}$	<i>Mickett et al.</i> [2004]

<sup>a</sup>The St. Lawrence Estuary is shown for comparison.

been argued to be valid for internal wave breaking, this suggests that internal waves may be an important contributor to mixing the inner basin of the Saguenay Fjord. Whether or not internal waves are the cause of the observed mixing, this relationship with our fitted parameters for *a* and *b* may be useful for parameterizing the diffusivity in the Saguenay Fjord when no other more advanced models or detailed observations are available.

#### 4.3.2. Other Hypotheses on Mixing

Given the narrowness of the fjord, narrower than the internal Rossby radius, another possible source of turbulence is the lateral friction with the rough sidewall cliffs. The formation of surface eddies accompanied by vertical shear velocities has been observed in the Saguenay and might also be present deeper in the water column, causing vertical mixing.

The increase of mixing by entrainment is not to be neglected as the Saguenay is never totally stagnant and intrusions at different depth contribute to mixing. However, *Seibert et al.* [1979] found that the kinetic energy of friction and entrainment of dense plumes in the outer basin of the Saguenay is not sufficient to explain the high renewal rates observed in the outer basin and tidal processes are necessary to carry energy into the deep basins.

#### 4.4. The Saguenay in a Broader Context

Deep waters of the Saguenay seem to be renewed at a rate significantly higher than other sill fjords (e.g., Loch Etive, Scotland [*Edwards and Edelsten*, 1977], Bonnefjord (part of Oslofjord), Norway [*Gade*, 1970; *Stigebrandt*, 2012], Hardangerfjord, Sognefjord, and other west coast Norwegian fjords [*Gade*, 1973]). The eddy diffusivity of the Saguenay is in fact larger than diffusivities observed in many other places but can still be comparable to some fjords with rough topography and large forcing (Table 3). The large tidal forcing, a distinguishing feature of the Saguenay Fjord, and the presence of the three sills definitely contribute to the large mixing rates which makes deep renewals possible every year.

### 5. Conclusion

Our results support the hypotheses of *Bourgault et al.* [2012a] concerning the timing and origin of the deep (winter) and intermediate (summer) renewals. However, the occurrence of a sudden circulation shift in winter and the presence of subsurface renewals are new contributions to the understanding of the renewal dynamics in the Saguenay Fjord.

Little was known about the factors that control the deep water inflows. This study provides new supporting evidence, that the complexity of the fjord renewals and inner circulation is dependent on the St. Lawrence Estuary dynamics. The Saguenay Fjord renewal mechanisms are distinct from most other fjord because of its being connected to an Estuary with large tides rather than directly to the coastal ocean. It can be concluded that while St. Lawrence runoff rate may contribute to variation of density at the sill, it is the combination of both tidal range and St. Lawrence estuarine circulation seasonal variation that are the more important mechanisms. The effects of wind forcing [*Bélanger*, 2003] on the circulation and renewal events were however not fully addressed and should be investigated further.

The mechanisms driving vertical mixing in the Saguenay inner basin are not yet clearly identified and understood but the significant relationship found between the turbulent diffusivity and the buoyancy frequency points in the direction of internal waves. New field measurements and process-oriented numerical studies are required to better understand the role of bottom and side friction, horizontal eddies, internal

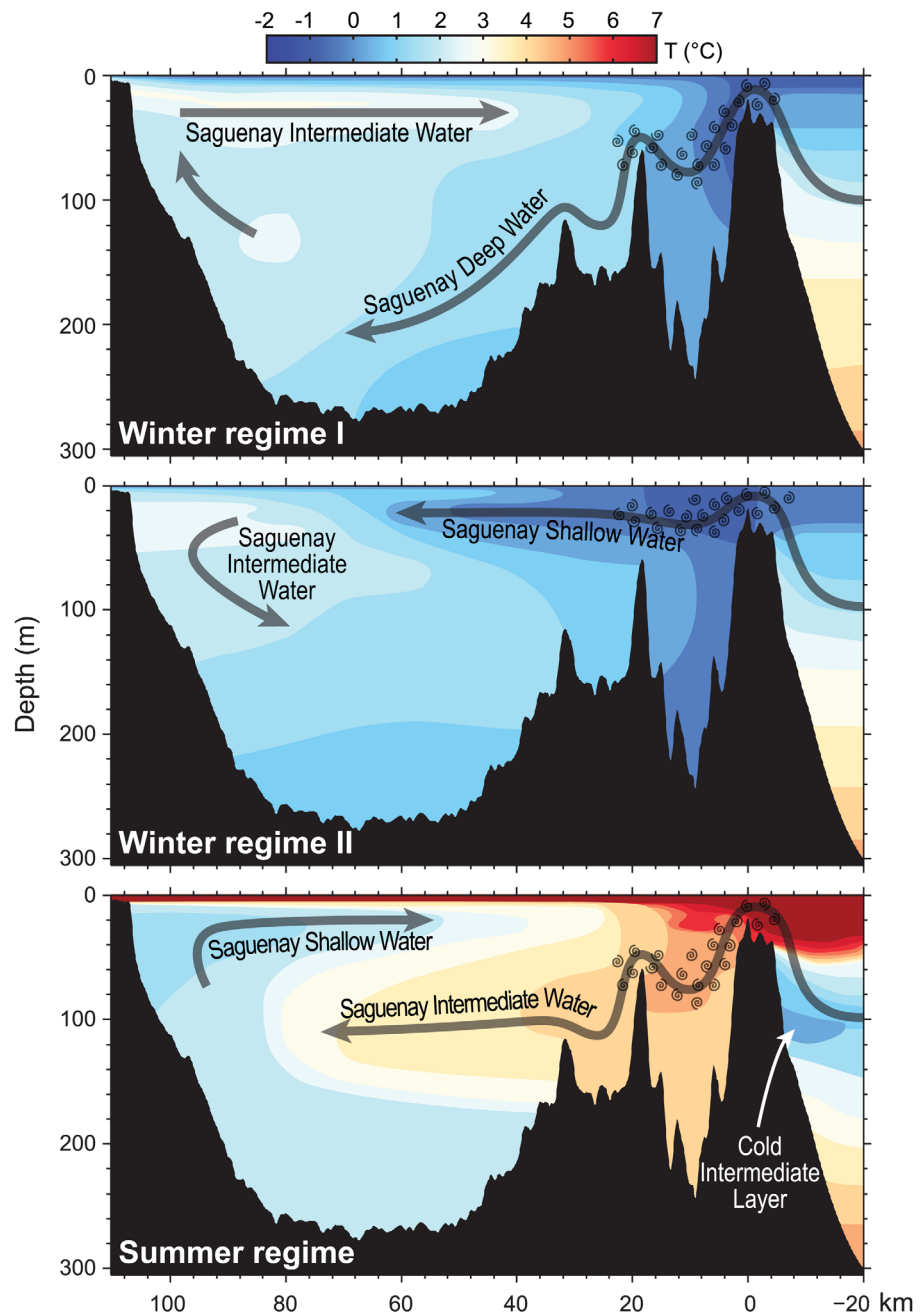


**Figure 13.** Schematic synthesis of the three types of renewal regimes in the Saguenay Fjord; deep renewals during (top) fall and early winter, (middle) mid or late winter subsurface renewals, and (bottom) intermediate renewals during summer.

tides, and sill processes in mixing the deep water. A relevant and feasible field experiment could be to sample turbulence profiles at a site closer to the sills region over the tidal cycle and at various phases of the spring-neap cycle.

The main results of this study, on the seasonal variability of water renewals and circulation, are summarized in Figure 13. The first part represents the deep renewals (SDW) occurring in fall and early winter. It is suggested that such dense water inflows displace the resident intermediate waters (SIW) upward, toward the return current. This mechanism may explain the warm pocket of water found at the head of the fjord in winter. Then, in the middle of winter, an abrupt change occurs in salinity at the sill, forcing a shift of the renewal circulation pattern whereby inflowing waters start to renew the inner basin at subsurface depths (SSW).

These intrusions may displace the resident waters downward, replacing the first 100 m of the water column (Figure 13). Finally, in summer, intermediate renewals (SIW) start to occur, bringing warmer waters inside the inner basin, and probably trapping the cold water from subsurface renewals (SSW) at the head of the fjord (Figure 13). As large mixing acts to decrease deep water density, these three renewal types can occur every year according to the St. Lawrence seasonal circulation showing an interannual variability in regard to their beginning time and duration.

#### Acknowledgments

This work was funded by the Natural Sciences and Engineering Research Council of Canada, the Canada Foundation for Innovation, Fisheries and Oceans Canada, and Québec-Océan. We are thankful to Sylvain Blondeau (Québec-Océan), Rémi Desmarais (IML), and Gilles Desmeules (ISMER) for the preparation, deployment, and recovery of the moorings. We are grateful to Nadia Ménard (Saguenay-St. Lawrence Marine Park) for transect data. Thanks to Pascal Guillot (Québec-Océan) for the data quality control and finally many thanks to Johanne Noël (St. Lawrence Global Observatory) for her work on the synthesis figure. All hydrographic and historical data used in this research are available through Oceanographic Data Management System (ODMS), Department of Fisheries and Oceans Canada (<http://slgo.ca/app-sgdo/en/accueil.html>) and all mooring data are available via Pascal Guillot ([pascal\\_guillot@uqar.ca](mailto:pascal_guillot@uqar.ca)).

#### References

- Allen, G. L., and J. H. Simpson (1998), Deep water inflows to Upper Loch Linnhe, *Estuarine Coastal Shelf Sci.*, *47*(4), 487–498.
- Arneborg, L., C. P. Erlandsson, B. Liljebladh, and A. Stigebrandt (2004a), The rate of inflow and mixing during deep-water renewal in a sill fjord, *Limnol. Oceanogr.*, *49*(3), 768–777.
- Arneborg, L., C. Janzen, B. Liljebladh, T. P. Rippeth, J. H. Simpson, and A. Stigebrandt (2004b), Spatial variability of diapycnal mixing and turbulent dissipation rates in a stagnant fjord basin, *J. Phys. Oceanogr.*, *34*(7), 1679–1691.
- Baschek, B., and W. J. Jenkins (2009), Gas ventilation of the Saguenay Fjord by an energetic tidal front, *Atmos. Ocean*, *47*(4), 308–318.
- Bélanger, C. (2003), Observation and modelling of a renewal event in the Saguenay Fjord, PhD thesis, 235 pp., Univ. du Qué. à Rimouski, Rimouski, Québec, Canada.
- Bourgault, D., P. S. Galbraith, and G. Winkler (2012a), Exploratory observations of winter oceanographic conditions in the Saguenay Fjord, *Atmos. Ocean*, *50*(1), 17–30.
- Bourgault, D., F. Cyr, P. S. Galbraith, and E. Pelletier (2012b), Relative importance of pelagic and sediment respiration in causing hypoxia in a deep estuary, *J. Geophys. Res.*, *117*, C08033, doi:10.1029/2012JC007902.
- Cottier, F. R., F. Nilssen, R. Skogseth, V. Tverberg, J. Skarohamar, and H. Svendsen (2010), Arctic fjords: A review of the oceanographic environment and dominant physical processes, *Geol. Soc. Spec. Publ.*, *344*(1), 35–50.
- Cyr, F., D. Bourgault, and P. S. Galbraith (2011), Interior versus boundary mixing of a cold intermediate layer, *J. Geophys. Res.*, *116*, C12029, doi:10.1029/2011JC007359.
- Cyr, F., D. Bourgault, P. S. Galbraith, and M. Gosselin (2015), Turbulent nitrate fluxes in the Lower St. Lawrence Estuary, Canada, *J. Geophys. Res. Oceans*, *120*, 2308–2330, doi:10.1002/2014JC010272.
- de Young, B., and S. Pond (1988), The deepwater exchange cycle in Indian arm, British Columbia, *Estuarine Coastal Shelf Sci.*, *26*(3), 285–308.
- Drainville, G. (1968), Le fjord du Saguenay: I. Contribution à l'océanographie, *Nat. Can.*, *95*(4), 809–855.
- Edwards, A., and D. J. Edelsten (1977), Deep water renewal of Loch Etive: A three basin Scottish Fjord, *Estuarine Coastal Mar. Sci.*, *5*(5), 575–595.
- Efron, B., and G. Gong (1983), A leisurely look at the bootstrap, the jackknife and cross-validation, *Am. Stat.*, *37*(1), 36–48.
- Farmer, D. M., and H. J. Freeland (1983), The physical oceanography of fjords, *Prog. Oceanogr.*, *12*(2), 147–219.
- Fer, I. (2006), Scaling turbulent dissipation in an arctic fjord, *Deep Sea Res., Part II*, *53*(1), 77–95.
- Fer, I., and K. Widell (2007), Early spring turbulent mixing in an ice-covered arctic fjord during transition to melting, *Cont. Shelf Res.*, *27*(15), 1980–1999.
- Gade, H. G. (1970), *Hydrographic Investigations in the Oslofjord: A Study of Water Circulation and Exchange Processes*, vol. 1, Report 24, Geophysical Institute Div. A, University of Bergen, Norway.
- Gade, H. G. (1973), Deep water exchanges in a Sill Fjord: A stochastic process, *J. Phys. Oceanogr.*, *3*(2), 213–219.
- Gade, H. G. (1986), Features of fjord and ocean interaction, in edited by B. G. Hurdle *The Nordic Seas*, pp. 183–190, Springer, N. Y.
- Gade, H. G., and A. Edwards (1980), Deep water renewal in fjords, in *Fjord Oceanography*, edited by H. J. Freeland, D. M. Farmer, and C. D. Levings, pp. 453–489, Plenum Press, N. Y.
- Galbraith, P. S. (2006), Winter water masses in the Gulf of St. Lawrence, *J. Geophys. Res.*, *111*, C06022, doi:10.1029/2005JC003159.
- Galbraith, P. S., J. Chassé, P. Nicot, C. Caverhill, D. Gilbert, B. Pettigrew, D. Lefavre, D. Brickman, L. Devine, and C. Lafleur (2015), Physical oceanographic conditions in the Gulf of St. Lawrence in 2014, *DFO Can. Sci. Advis. Sec. Res. Doc. 2015/032*, v + 82 pp. Fisheries and Oceans Canada, Canadian Science Advisory Secretariat, Ottawa, ON.
- Gargett, A. E., and G. Holloway (1984), Dissipation and diffusion by internal wave breaking, *J. Mar. Res.*, *42*(1), 15–27.
- Geyer, W. R., and G. A. Cannon (1982), Sill processes related to deep water renewal in a fjord, *J. Geophys. Res.*, *87*(C10), 7985–7996.
- Guillot, P. (2011), Rapport de traitement des données de l'ADCP RDI 0333 du mouillage sagwin01-2011, Draft version, technical report, Qué.-Océan, Univ. Laval, Québec, Canada.
- Inall, M. E., and P. A. Gillibrand (2010), The physics of mid-latitude fjords: a review, *Geol. Soc. Spec. Publ.*, *344*(1), 17–33.
- Inall, M. E., and T. P. Rippeth (2002), Dissipation of tidal energy and associated mixing in a wide fjord, *Environ. Fluid Mech.*, *2*(3), 219–240.
- Janes, D. C. (2008), Sill processes in the Saguenay Fjord, master's thesis, 79 pp., Mem. Univ., St. John's, Canada.
- Lavoie, D., Y. Simard, and F. J. Saucier (2000), Aggregation and dispersion of krill at channel heads and shelf edges: The dynamics in the Saguenay-St. Lawrence Marine Park, *Can. J. Fish. Aquat. Sci.*, *57*(9), 1853–1869.
- Liungman, O., L. Rydberg, and C. G. Göransson (2001), Modeling and observations of deep water renewal and entrainment in a Swedish Sill Fjord, *J. Phys. Oceanogr.*, *31*(12), 3401–3420.
- Loucks, R. H., and R. E. Smith-Sinclair (1975), The physical oceanography of the Saguenay Fjord, technical report, Chem. Ocean. Div., Bedford Inst. of Oceanogr., Dartmouth, NS, Canada.
- Mellor, G. L., and T. Yamada (1982), Development of a turbulence closure model for geophysical fluid problems, *Rev. Geophys.*, *20*(4), 851–875.
- Mickett, J. B., M. C. Gregg, and H. E. Seim (2004), Direct measurements of diapycnal mixing in a fjord reach—Puget Sound's Main Basin, *Estuarine Coastal Shelf Sci.*, *59*(4), 539–558.
- Mortensen, J., J. Bendtsen, K. Lennert, and S. Rysgaard (2014), Seasonal variability of the circulation system in a west Greenland tidewater outlet glacier fjord, Godthåbsfjord (64°N), *J. Geophys. Res. Earth Surf.*, *119*, 2591–2603, doi:10.1002/2014JF003267.
- Osborn, T. R. (1980), Estimates of the local rate of vertical diffusion from dissipation measurements, *J. Phys. Oceanogr.*, *10*(1), 83–89.
- Saucier, F. J., and J. Chassé (2000), Tidal circulation and buoyancy effects in the St. Lawrence Estuary, *Atmos. Ocean*, *38*(4), 505–556.
- Saucier, F. J., F. Roy, S. Senneville, G. Smith, D. Lefavre, B. Zakardjian, and J.-F. Dumais (2009), Modélisation de la circulation dans l'estuaire et le Golfe du Saint-Laurent en réponse aux variations du débit deau douce et des vents, *J. Water Sci.*, *22*(2), 159–176.

- Schafer, C. T., J. N. Smith, and R. Côté (1990), The Saguenay Fjord: A major tributary to the St. Lawrence Estuary, in *Oceanography of a Large-Scale Estuarine System, the St. Lawrence, Coastal Estuarine Stud.*, vol. 39, edited by M. I. El-Sabh and N. Silverberg, pp. 378–420, Springer, N. Y.
- Sciascia, R., C. Cenedese, D. Nicoli, P. Heimbach, and F. Straneo (2014), Impact of periodic intermediary flows on submarine melting of a Greenland glacier, *J. Geophys. Res. Oceans*, 119(10), 7078–7098, doi:10.1002/2014JC009953.
- Seibert, G. H., R. W. Trites, and S. J. Reid (1979), Deepwater exchange processes in the Saguenay Fjord, *J. Fish. Board Can.*, 36(1), 42–53.
- Smethie, W. M. J. (1980), Estimation of vertical mixing rates in fjords using naturally occurring radon-222 and salinity as tracers, in *Fjord Oceanography*, edited by H. J. Freeland, D. M. Farmer, and C. D. Levings, pp. 241–249, Plenum Press, N. Y.
- Smith, G. C., F. J. Saucier, and D. Straub (2006), Response of the lower St. Lawrence Estuary to external forcing in winter, *J. Phys. Oceanogr.*, 36(8), 1485–1501.
- Stacey, M. W., and Y. Gratton (2001), The energetics and tidally induced reverse renewal in a two-silled fjord, *J. Phys. Oceanogr.*, 31(6), 1599–1615.
- Stacey, M. W., S. Pond, and Z. P. Nowak (1995), A numerical model of the circulation in knight inlet, British Columbia, Canada, *J. Phys. Oceanogr.*, 25(6), 1037–1062.
- Stigebrandt, A. (1976), Vertical diffusion driven by internal waves in a sill fjord, *J. Phys. Oceanogr.*, 6(4), 486–495.
- Stigebrandt, A. (1990), On the response of the horizontal mean vertical density distribution in a fjord to low-frequency density fluctuations in the coastal water, *Tellus, Ser. A*, 42(5), 605–614.
- Stigebrandt, A. (2012), Hydrodynamics and circulation of fjords, in *Encyclopedia of Lakes and Reservoirs*, edited by L. Bengtsson, R. W. Herschy, and R. W. Fairbridge, pp. 327–344, Springer Science, Dordrecht, Netherlands, doi:10.1007/978-1-4020-4410-6.
- Stigebrandt, A., and J. Aure (1989), Vertical mixing in basin waters of fjords, *J. Phys. Oceanogr.*, 19(7), 917–926.
- Stigebrandt, A., and O. Kalén (2013), Improving oxygen conditions in the deeper parts of Bornholm Sea by pumped injection of winter water, *Ambio*, 42(5), 587–595.
- Sundby, B., and D. H. Loring (1978), Geochemistry of suspended particulate matter in the Saguenay Fjord, *Can. J. Earth Sci.*, 15(6), 1002–1011.
- Sutherland, D. A., F. Straneo, and R. S. Pickart (2014), Characteristics and dynamics of two major Greenland glacial fjords, *J. Geophys. Res. Oceans*, 119(6), 3767–3791.
- Svensson, T. (1980), *Tracer Measurement of Mixing in the Deep Water of a Small, Stratified Sill Fjord*, *Fjord Oceanography*, edited by H. J. Freeland, D. M. Farmer, and C. D. Levings, pp. 233–240, Plenum Press, N. Y.
- Taylor, G. B. (1975), Saguenay River sections from fifteen cruises, technical report, Data Series BI-D-75-2, Bedford Inst. of Oceanogr., Dartmouth, NS, Canada.
- Therriault, J. C., and G. Lacroix (1975), Penetration of the deep layer of the Saguenay Fjord by surface waters of the St. Lawrence Estuary, *J. Fish. Board Can.*, 32(12), 2373–2377.
- Therriault, J. C., R. De Ladurantaye, and R. G. Ingram (1984), Particulate matter exchange across a fjord sill, *Estuarine Coastal Shelf Sci.*, 18(1), 51–64.
- Xie, H., C. Aubry, S. Bélanger, and G. Song (2012), The dynamics of absorption coefficients of CDOM and particles in the St. Lawrence estuarine system: Biogeochemical and physical implications, *Mar. Chem.*, 128, 44–56.